doi:10.1093/plphys/kiab099 PLANT PHYSIOLOGY 2021: 187: 2192–2208

Plant Physiology®

Research Article

Subunit E isoform 1 of vacuolar H$^+$-ATPase OsVHA enables post-Golgi trafficking of rice seed storage proteins

Jianping Zhu ,[1,‡] Yulong Ren ,[2,‡] Yuanyan Zhang,[1,‡] Jie Yang ,[3] Erchao Duan ,[1] Yunlong Wang,[1] Feng Liu ,[4] Mingming Wu ,[1] Tian Pan ,[1] Yongfei Wang ,[1] Tingting Hu ,[1] Yuanyuan Hao,[1] Xuan Teng,[1] Xiaopin Zhu,[1] Jie Lei,[1] Ruonan Jing ,[1] Yanfang Yu,[1] Yinglun Sun,[1] Xiuhao Bao ,[1] Yiqun Bao ,[4] Yihua Wang [1,†] and Jianmin Wan [1,2,*,†]

1 State Key Laboratory of Crop Genetics and Germplasm Enhancement, Jiangsu Plant Gene Engineering Research Center, Nanjing Agricultural University, Nanjing 210095, China
2 National Key Facility for Crop Resources and Genetic Improvement, Institute of Crop Sciences, Chinese Academy of Agricultural Sciences, Beijing 100081, PR China
3 Institute of Food Crops, Jiangsu Academy of Agricultural Sciences, Nanjing 210014, China
4 College of Life Sciences, Nanjing Agricultural University, Nanjing 210095, PR China

*Author for communication: wanjm@njau.edu.cn, wanjianmin@caas.cn
†Senior authors.
‡These authors contributed equally to this work (J.Z., Y.R., Y.Z.).

J.W., Y.H.W., Y.R., and J.Z. designed the research. Y.Z., E.D., Y.W., F.L., M.W., T.P., Y.F.W., T.H., Y.H., X.T., X.Z., J.L., R.J., Y.Y., Y.S., and X.B. performed the experiments. J.Z. wrote the article. W.J., Y.B., Y.H.W., and J.Y. revised the article. All authors read and approved the final article.
The author responsible for distribution of materials integral to the findings presented in this article in accordance with the policy described in the Instructions for Authors (https://academic.oup.com/plphys/pages/general-instructions) is: Jianmin Wan (wanjm@njau.edu.cn, wanjianmin@caas.cn).

Abstract

Dense vesicles (DVs) are Golgi-derived plant-specific carriers that mediate post-Golgi transport of seed storage proteins in angiosperms. How this process is regulated remains elusive. Here, we report a rice (*Oryza sativa*) mutant, named *glutelin precursor accumulation8* (*gpa8*) that abnormally accumulates 57-kDa proglutelins in the mature endosperm. Cytological analyses of the *gpa8* mutant revealed that proglutelin-containing DVs were mistargeted to the apoplast forming electron-dense aggregates and paramural bodies in developing endosperm cells. Differing from previously reported *gpa* mutants with post-Golgi trafficking defects, the *gpa8* mutant showed bent Golgi bodies, defective trans-Golgi network (TGN), and enlarged DVs, suggesting a specific role of GPA8 in DV biogenesis. We demonstrated that *GPA8* encodes a subunit E isoform 1 of vacuolar H$^+$-ATPase (OsVHA-E1) that mainly localizes to TGN and the tonoplast. Further analysis revealed that the luminal pH of the TGN and vacuole is dramatically increased in the *gpa8* mutant. Moreover, the colocalization of GPA1 and GPA3 with TGN marker protein in *gpa8* protoplasts was obviously decreased. Our data indicated that OsVHA-E1 is involved in endomembrane luminal pH homeostasis, as well as maintenance of Golgi morphology and TGN required for DV biogenesis and subsequent protein trafficking in rice endosperm cells.

Received January 15, 2021. Accepted February 8, 2021. Advance access publication February 24, 2021

Introduction

Rice (*Oryza sativa*) seeds accumulate large amounts of storage proteins, including glutelins, prolamins, and α-globulin, which supply nutrients for seed germination and seedling growth (Yamagata and Tanaka, 1986). Up to 80% of total seed storage proteins are made up of glutelins, which are important protein sources for human consumption. Seed storage proteins deposit in two types of protein bodies (PBs): PBI and PBII (Bechtel and Juliano, 1980; Pernollet and Mossé, 1983). PBI mainly accumulates prolamins. In electron microscopy observation, PBI has a low electron density and a round shape with a diameter of 1–2 μm. The surface is surrounded by a layer of rough endoplasmic reticulum (RER; ribosomes are easy to see on its surface; Tanaka et al., 1980; Ogawa et al., 1987). PBII has a high electron density and is irregular in shape, with a diameter of about 3–4 μm. It mainly accumulates glutelins and globulins (Bechtel and Juliano, 1980; Tanaka et al., 1980). Glutelins are synthesized as 57-kDa precursors on the RER and transported to PBIIs by the dense vesicle (DV)-mediated post-Golgi trafficking pathway or endoplasmic reticulum (ER)-derived precursor-accumulating compartments that bypass the Golgi apparatus (Yamagata et al., 1982; Krishnan et al., 1986; Takemoto et al., 2002; Takahashi et al., 2005; Liu et al., 2013; Ren et al., 2014). Within PBIIs, proglutelins are cleaved into mature subunits by VACUOLAR-PROCESSING ENZYME1 (OsVPE1)/GLUTELIN PRECURSOR3 (GLUP3; Wang et al., 2009; Kumamaru et al., 2010).

DVs are the important carriers containing a single membrane with a diameter of 100–200 nm and are responsible for transporting a variety of seed storage proteins in angiosperms, such as faba bean (*Vicia faba*), pea (*Pisum sativum*), rice (*O. sativa*), and Arabidopsis (*Arabidopsis thaliana*; Krishnan et al., 1986; Hohl et al., 1996; Hinz et al., 1999; Otegui et al., 2006). The vacuolar storage proteins first aggregate at the cis-Golgi, being transported through the Golgi, and budded from the trans-Golgi network (TGN) in the form of DVs (Hillmer et al., 2001; Hinz et al., 2007; Wang et al., 2012). It is generally believed that DVs fuse with prevacuolar compartments (PVCs) and then the PVCs fuse with protein storage vacuoles (PSVs) to complete the transportation of cargos (Otegui et al., 2006; Shen et al., 2011). However, DVs appear to directly fuse with PSVs to transport proglutelins in rice endosperm cells (Liu et al., 2013; Ren et al., 2020).

Angiosperm seeds with over-accumulated precursors of storage proteins, such as globulins and albumins in Arabidopsis (*A. thaliana*) and glutelins in rice (*O. sativa*), are excellent genetic resources to dissect the vacuolar transport pathway (Shimada et al., 2003; Cui et al., 2014; Ren et al., 2014, 2020; Wang et al., 2016). In Arabidopsis, a series of factors, including VACUOLAR SORTING RECEPTOR1 (AtVSR1), MONENSIN SENSITIVITY1-CALCIUM CAFFEINE ZINC SENSITIVITY1 (AtMON-AtCCZ1), VACUOLAR PROTEIN SORTING9A (AtVPS9A), Na^+/H^+ ANTIPORTER5/6 (AtNHX5/6), and MEDIUM SUBUNIT OF ADAPTOR PROTEIN COMPLEX4 (AtAP4M) are required for the post-Golgi trafficking of storage proteins (Shimada et al., 2003; Cui et al., 2014; Ebine et al., 2014; Reguera et al., 2015; Fuji et al., 2016). In rice, at least five genes have been shown to regulate DV-mediated post-Golgi proglutelin trafficking events. GLUTELIN PRECURSOR ACCUMULATION3 (GPA3), a plant-specific kelch-repeat domain-containing protein, is postulated to recruit guanine–nucleotide exchange factor GPA2/GLUP6/OsVPS9A, which in turn activates a small GTPase GPA1/GLUP4/RAS-RELATED PROTEIN RAB-5A (OsRab5a; Wang et al., 2010; Fukuda et al., 2011, 2013; Liu et al., 2013; Ren et al., 2014). The GPA3, GPA2, and GPA1 proteins form a functional complex to regulate vacuolar trafficking of proglutelins (Ren et al., 2014). *GLUTELIN PRECURSOR ACCUMULATION6* (*GPA6*)/Na^+/H^+ *ANTIPORTER5* (*OsNHX5*) encoding the Na^+/H^+ antiporter functions in endomembrane luminal pH homeostasis (Zhu et al., 2019). Recently, Ren et al. (2020) reported that GPA5 functions as a plant-specific effector of Rab5a required for mediating tethering and membrane fusion of DVs with PSVs. Mutations of these genes all resulted in the missorting of DVs to the apoplast. Despite these advances, the regulatory mechanisms underlying the DV-mediated post-Golgi trafficking remain largely unknown in plants, especially DV biogenesis.

Vacuolar H^+-ATPases (V-ATPases) conserved in eukaryotes consist of two subcomplexes (V_1 and V_0; Nishi and Forgac, 2002; Schumacher and Krebs, 2010). The cytosolic V_1 subcomplex includes eight subunits (A–H) and is responsible for ATP hydrolysis. The membrane-integrated V_0 consisting of six subunits (a, c, c′, c″, d, e) is responsible for proton translocation (Nishi and Forgac, 2002; Schumacher and Krebs, 2010). V-ATPase uses the energy released by ATP hydrolysis to pump protons into endomembrane compartments to maintain acidic pH compared with the cytosol. In addition, the membrane potential generated by V-ATPase is required for secondary transport (Schumacher and Krebs, 2010). In plants, V-ATPases are essential for cellular pH and ion homeostasis. They play important roles in various cellular processes, such as pH homeostasis (Luo et al., 2015), vesicular trafficking (Dettmer et al., 2006), cell expansion (Schumacher et al., 1999), stomatal aperture (Zhang et al., 2013), salt tolerance (Batelli et al., 2007), and plant growth and development (Padmanaban et al., 2004; Dettmer et al., 2005; Strompen et al., 2005; Zhou et al., 2016). AtVHA-E1 is required for Golgi organization and vacuole function (Strompen et al., 2005). In addition, *PREMATURE LEAF SENESCENCE1* (*OsPLS1*)/*OsVHA-A1* is closely associated with leaf senescence and seed dormancy (Yang et al., 2016). However, the functions of V-ATPases in plants are still to be addressed.

In this study, we reported the functional characterization of a rice *gpa8* mutant that accumulated a large amount of proglutelins in the endosperm. Cytological observation revealed that the DV-mediated post-Golgi trafficking was defective in the *gpa8* mutant. We demonstrated that *GPA8* encodes a subunit E isoform 1 of vacuolar H^+-ATPase (OsVHA-E1). The luminal pH of TGN and vacuole is increased in the *gpa8* mutant. Our data indicated that OsVHA-E1 is involved in endomembrane luminal pH homeostasis and DV-mediated proglutelin vacuolar trafficking in rice.

Results

Phenotypic characterization of the *gpa8-1* mutant

In order to better dissect the glutelin trafficking pathway in rice, we isolated two allelic proglutelin overaccumulation mutants (57H mutant, 57-kDa proglutelin overaccumulation mutants) named *gpa8-1* and *gpa8-2*. *gpa8-2* exhibited a seedling lethal phenotype (Figure 1A). The *gpa8-1* mutant exhibited a lesion-mimic phenotype in basal leaves of 1-month-old seedlings and the symptoms became more severe at the maturation stage, Moreover, *gpa8-1* mature plants were much shorter than the wild-type (WT). Tiller numbers were also significantly reduced. These results suggested that GPA8 is crucial for plant growth and development (Supplemental Figure S1). After grain filling, *gpa8-1* mutant endosperm appeared floury compared with transparent WT endosperm (Figure 1B). Scanning electron microscopy analysis revealed that *gpa8-1* endosperm comprised round, loosely packaged compound starch granules instead of the tightly packaged, crystal-like structures observed in the WT (Figure 1, C and D). In addition, 1,000-grain weight was significantly decreased in the *gpa8-1* mutant (Supplemental Table S1). Compared with WT, the *gpa8-1* mutant accumulated approximately two-fold higher levels of 57-kDa proglutelin, accompanied by significant reductions in 40-kDa acidic and 20-kDa basic subunits typical of the mature glutelins (Figure 1, E and F; Supplemental Figure S2). Storage protein accumulation in wild-type and *gpa8-1* mutant seeds began at ~6 d after flowering (DAF), but the *gpa8-1* seeds deposited higher amounts of 57-kDa proglutelin than the WT seeds from ~12 DAF (Supplemental Figure S3). The expression of representative genes coding for storage proteins in 12 DAF endosperm showed no obvious change between WT and the *gpa8-1* mutant (Supplemental Figure S4). We compared the protein levels of ER lumen BINDING PROTEIN1 (BiP1) and PROTEIN DISULFIDE ISOMERASE1-1 (PDI1-1) to assess whether the ER was affected in the mutant, but there was no difference between mutant and WT seeds (Figure 1F, Supplemental Figure S2B). These results suggested that the *gpa8-1* mutant was defective in trafficking of proglutelins, possibly after the ER exit process.

Glutelins are missorted in *gpa8-1* mutant endosperm cells

To obtain a view of glutelin deposition, we prepared semi-thin sections (1 μm) of the WT and *gpa8-1* mutant endosperm at 12 DAF. Coomassie blue staining showed that abnormal protein-filled structures indicated by red arrowheads were readily observed in the *gpa8-1* mutant (Supplemental Figure S5), which resembled paramural bodies (PMBs) in *gpa1/glup4*, *gpa2/glup6*, *gpa3*, *gpa5*, and *gpa6* genotypes (Wang et al., 2010; Fukuda et al., 2011, 2013; Liu et al., 2013; Ren et al., 2014, 2020; Zhu et al., 2019). Immunofluorescence experiments using specific antibodies against glutelins and prolamins in the 12-DAF endosperm showed that the PMB structures were abnormally filled with glutelins (Figure 2, A–H). The PBIIs were smaller in the *gpa8-1* mutant, whereas the PBIs were almost the same size as the WT (Figure 2, I and J; Supplemental Figures S6 and S7). In addition, α-globulin was also partially transported to the PMBs in *gpa8-1* (Supplemental Figure S8). Consistent with the defects in proglutelin and α-globulin trafficking, pectins labeled with the JIM7 antibody were accumulated within the PMBs in the mutant rather than displaying an even distribution along the cell wall as in the WT (Supplemental Figure S9; Chebli et al., 2012). These results indicated that glutelins, α-globulin, and certain cell wall components were missorted to the apoplast.

DV biogenesis and trafficking were defective in the *gpa8-1* mutant

In order to further clarify the origin and the formation of PMBs in the *gpa8-1* mutant, we initiated transmission electron microscopy studies. We observed irregularly shaped PBIIs and round spherical PBIs in the WT endosperm cells (Figure 3A), but the PBIIs were smaller in the *gpa8-1* mutant (Figure 3B). WT endosperm cells showed normal morphologies of Golgi and TGN (Figure 3C), but the Golgi stacks were severely bent and fragmented in the mutant and contained electron-dense deposits (Figure 3D). Abnormal clustering of many Golgi bodies in the mutant (Figure 3, E and F) was confirmed by immunofluorescence labeling with the JIM 84 antibody (Supplemental Figure S10; Kaida et al., 2008). The number of TGN bodies was reduced in the *gpa8-1* mutant (16.5 ± 3.3 per Golgi stack [$n = 30$] in the WT versus 7.8 ± 1.5 per Golgi stack [$n = 35$] in the *gpa8-1* mutant).

Proglutelins are delivered to the PBIIs via the DV-mediated trafficking pathway (Krishnan et al., 1986). A large number of DVs were surrounded by bent Golgi apparatus and failed to reach the TGN in the *gpa8-1* mutant (Figure 3, D–F). The diameters of DVs in the vicinity of Golgi apparatus were increased in the *gpa8-1* mutant (157.24 ± 37.63 nm [$n = 42$] in the WT vs. 295.57 ± 40.36 nm [$n = 49$] in the *gpa8-1* mutant). Compared with the WT, numerous DVs aggregated around the Golgi to form clusters in the cytosol in the *gpa8-1* mutant (Figure 3G) with wider variation in size and electron density. In addition, large amounts of DVs were mistargeted to around the cell wall in the mutant compared with WT (Figure 3H). Interestingly, these DVs could fuse with the plasma membrane and cargos were transported to the apoplast (Figure 3, I and J), resulting in the formation of the complex PMBs (Figure 3, K and L). Immunoelectron microscopy was performed to establish the subcellular localization of glutelins. Compared with the WT, glutelins were found in large clusters of DVs in the cytosol and PMBs in the mutant. Only a small portion of glutelins was transported to the PBIIs in *gpa8-1* (Figure 4, A–F). These results indicated that DV biogenesis and trafficking were defective in the *gpa8-1* mutant, leading to the formation of enlarged and clustered DVs, complex PMBs, and smaller PBIIs.

Map-based cloning of *GPA8*

The *gpa8-1* mutant was isolated from an *N*-methyl-N-nitrosourea (MNU)-treated population of *japonica* variety Ninggeng 1. Genetic analysis revealed that the mutant phenotype was inherited as a single nuclear recessive mutation (Supplemental

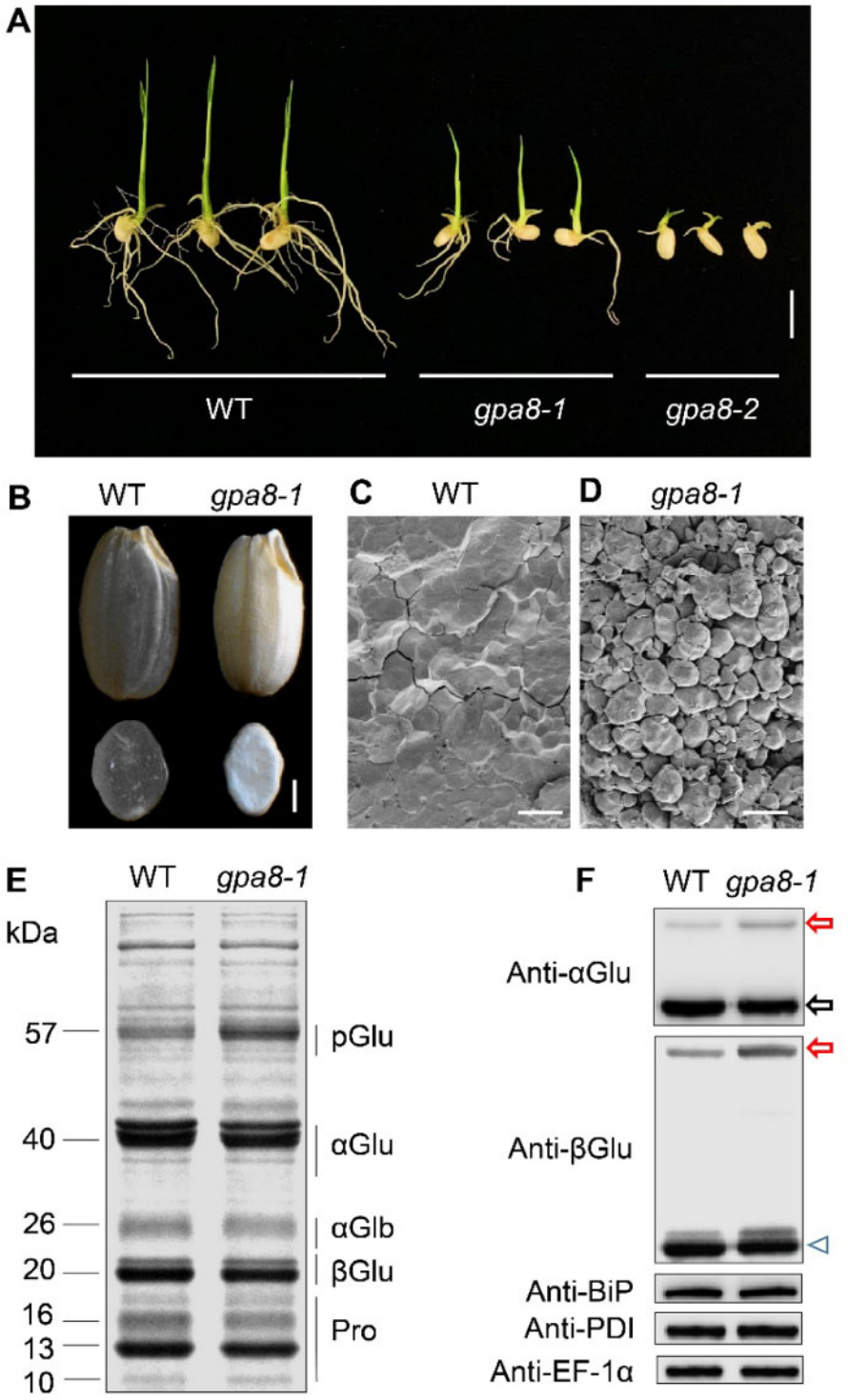

Figure 1 Characterization of the *gpa8* mutant. A, Images of WT (*japonica* variety Ninggeng 1), *gpa8-1* and *gpa8-2* seedlings grown for 6 d. Bars = 1 cm. B, Transverse sections of representative WT and *gpa8-1* mutant dry seeds. Bars = 1 mm. C and D, Scanning electron microscopy images of transverse sections of WT (C) and *gpa8-1* mutant (D) seeds. Bars = 10 μm. E, sodium dodecyl sulfate-polyacrylamide gel electrophoresis (SDS-PAGE) profiles of total seed storage proteins of WT and the *gpa8-1* mutant. pGlu, 57-kDa proglutelins; αGlu, 40-kDa glutelin acidic subunits; αGlb, 26-kDa α-globulin; βGlu, 20-kDa glutelin basic subunits; Pro, prolamins. F, Immunoblot analysis of glutelins and molecular chaperones BiP1 and PDI1-1. Arrowhead represents the glutelin basic subunits. Arrows indicate the 57-kDa proglutelins (red) and the glutelin acidic subunits (black). EF-1α was used as the loading control.

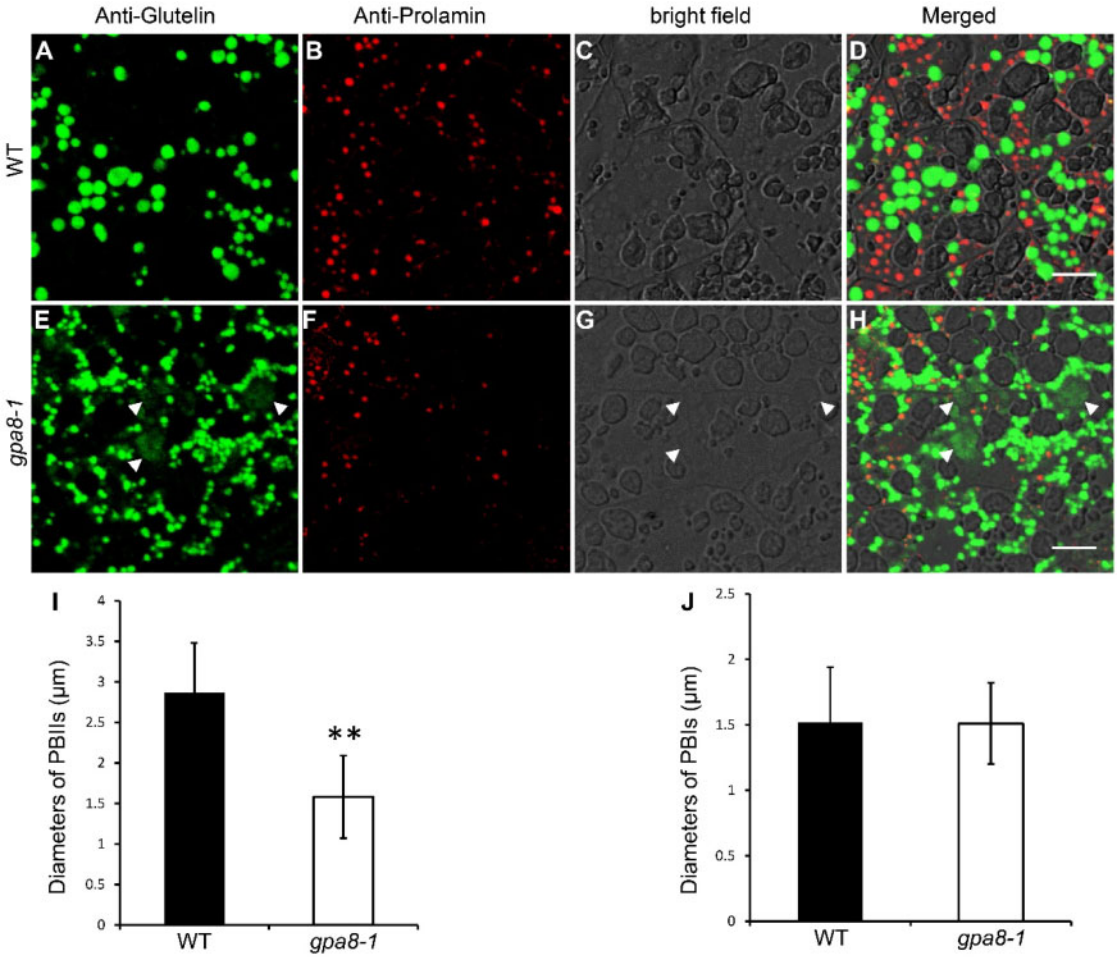

Figure 2 Immunofluorescence microscopy of protein bodies in subaleurone cells of WT and the *gpa8-1* mutant. A–H, Immunofluorescence microscopy images of storage proteins in WT (A–D) and *gpa8-1* (E–H) 12 DAF seeds. A and E, Secondary antibodies conjugated with Alexa fluor 488 (green) were used to trace the antigens recognized by anti-glutelin antibodies. B and F, Secondary antibodies conjugated with Alexa fluor 555 (red) were used to trace antigens recognized by the anti-prolamin antibodies. D and H, Merged images. White arrowheads in (E, G, and H) indicate the PMB structures. Bars = 10 μm (A–H). I and J, Statistical analysis of the diameters of PBIIs (I) and PBIs (J). Green and red protein bodies indicate PBIIs and PBIs, respectively. Values are means ± SD. $^{**}P < 0.01$ ($n > 230$, Student's t test).

Table S2). For map-based cloning, we crossed the *gpa8-1* mutant with the *indica* variety N22 and isolated 506 recessive F_2 individuals. The *GPA8* locus was initially mapped to chromosome 1 and further fine-mapped to a 59-kb genomic region (Figure 5A). DNA sequencing revealed a 2-bp deletion at the beginning of the fifth intron of *LOC_Os01g46980*, generating a premature stop codon that led to a putatively translated product of 222 amino acids (Figure 5B). In *gpa8-2*, a single nucleotide substitution in the first exon of *LOC_Os01g46980* caused a premature stop codon that led to a putatively truncated product with only 10 amino acids, resulting in a seedling lethal phenotype. Complementation experiment was made with the entire coding region of *LOC_Os01g46980* driven by the *UBIQUITIN* promoter. All positive transgenic lines rescued the *gpa8-1* mutant phenotypes, including the lesion-mimic leaves, floury endosperm appearance, amount of proglutelins, and pattern of deposited storage proteins (Figure 5, C–F; Supplemental Figure S11). In addition, *clustered regularly interspaced short palindromic repeats (CRISPR)/Cas9 alleles* (the 20-bp gene-specific target sequence in the fourth exon) showed similar seed phenotypes with *gpa8-1* (Supplemental Figure S12), while *CRISPR-alleles* exhibited a little more severe phenotypes than *gpa8-1* in vegetative stages, such as lesion mimic in basal leaves and tiller numbers. Therefore, *LOC_Os01g46980* is the responsible gene for *gpa8* phenotypes. Moreover, *gpa8-2* is most probably a knockout mutant of *LOC_Os01g46980*, while *gpa8-1* and the *CRISPR alleles* are knockdown mutants of *LOC_Os01g46980*.

GPA8 encodes subunit E1 of vacuolar H^+-ATPase

GPA8 encodes a subunit E isoform 1 (VHA-E1) of vacuolar H^+-ATPase that is homologous with AtVHA-E1, which contains a vATP-synt_E domain (Supplemental Figure S13A). We named *GPA8* as *OsVHA-E1*. Phylogenetic analysis indicated that genes homologous to *OsVHA-E1* exist in other eukaryotes and that the rice genome has two other isoforms of subunit E of vacuolar H^+-ATPase (*OsVHA-E2*, *LOC_Os05g40230* and *OsVHA-E3*, *LOC_Os01g12260*; Supplemental Figures S13, B and S14). Reverse transcription quantitative PCR (RT-qPCR)

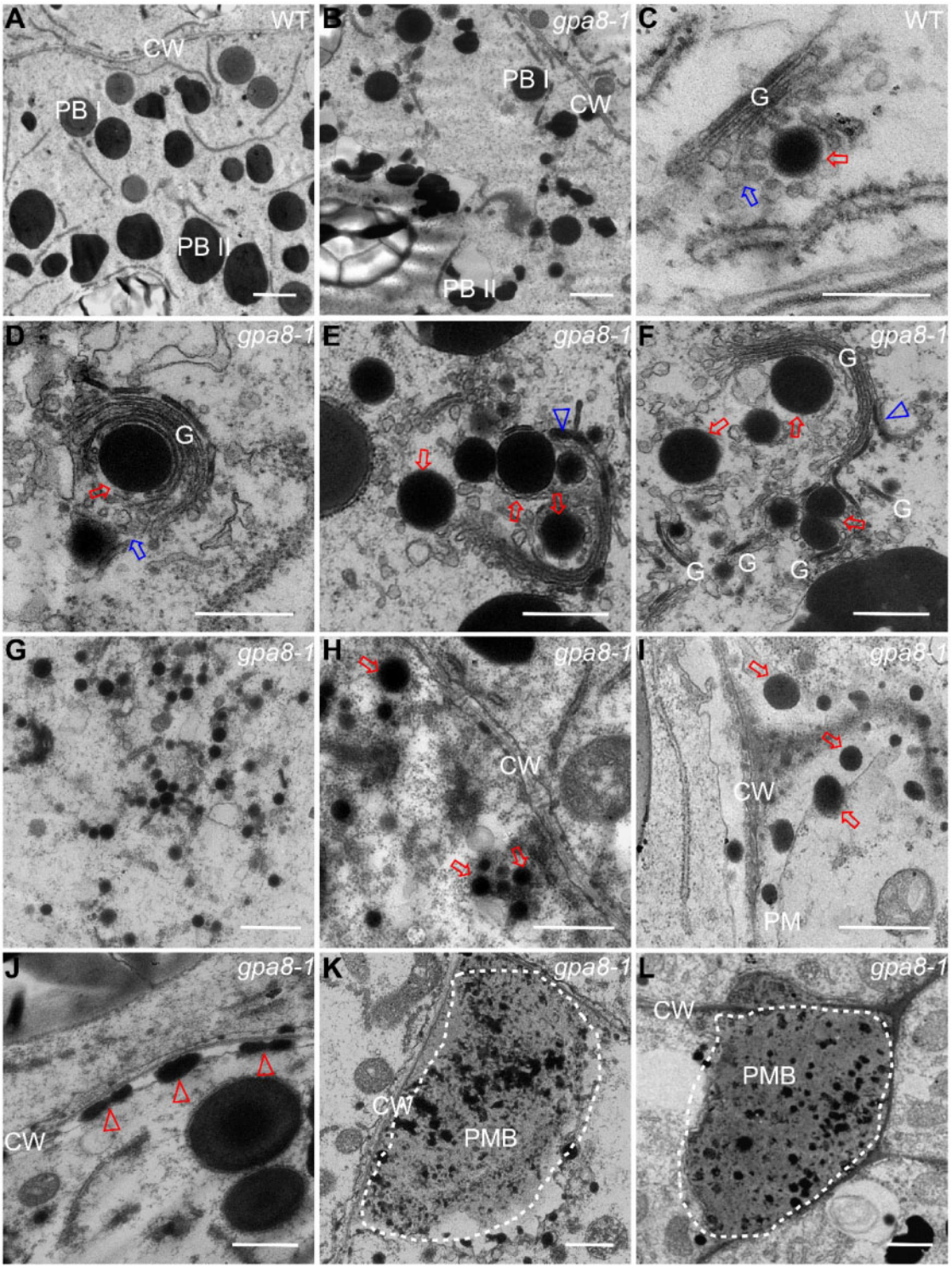

Figure 3 Ultrastructure of subaleurone cells of developing endosperm of WT and the *gpa8-1* mutant. A and B, Two types of protein bodies were observed in WT (A) and *gpa8-1* mutant (B) endosperm. Irregular and round shape protein bodies indicate PBIIs and PBIs, respectively. Bars = 2 μm. CW, cell wall. C and D, Golgi apparatus in WT (C) and *gpa8-1* mutant (D) endosperm cells. G, Golgi apparatus. Red arrows indicate DVs; blue arrows indicate TGN bodies. Bars = 300 nm. E and F, Different kinds of abnormal Golgi apparatus in *gpa8-1*. Large clusters of DVs aggregated around the Golgi apparatus in the *gpa8-1* mutant. Blue arrowheads indicate abnormal electron-dense materials in Golgi apparatus. Bars = 600 nm. G, Large clusters of DVs in the cytosol. Bars = 1 μm. H, Numerous DVs accumulate near the PM in the *gpa8-1* mutant. Bars = 1 μm. I and J, Electron micrographs showing that DVs can fuse with the PM (I) and release their contents into the apoplast forming electron-dense granules (arrowheads) (J). Bars = 1 μm. K and L, The PMB structures in 12 DAF endosperm cells (dotted boxes). Bars = 1 μm.

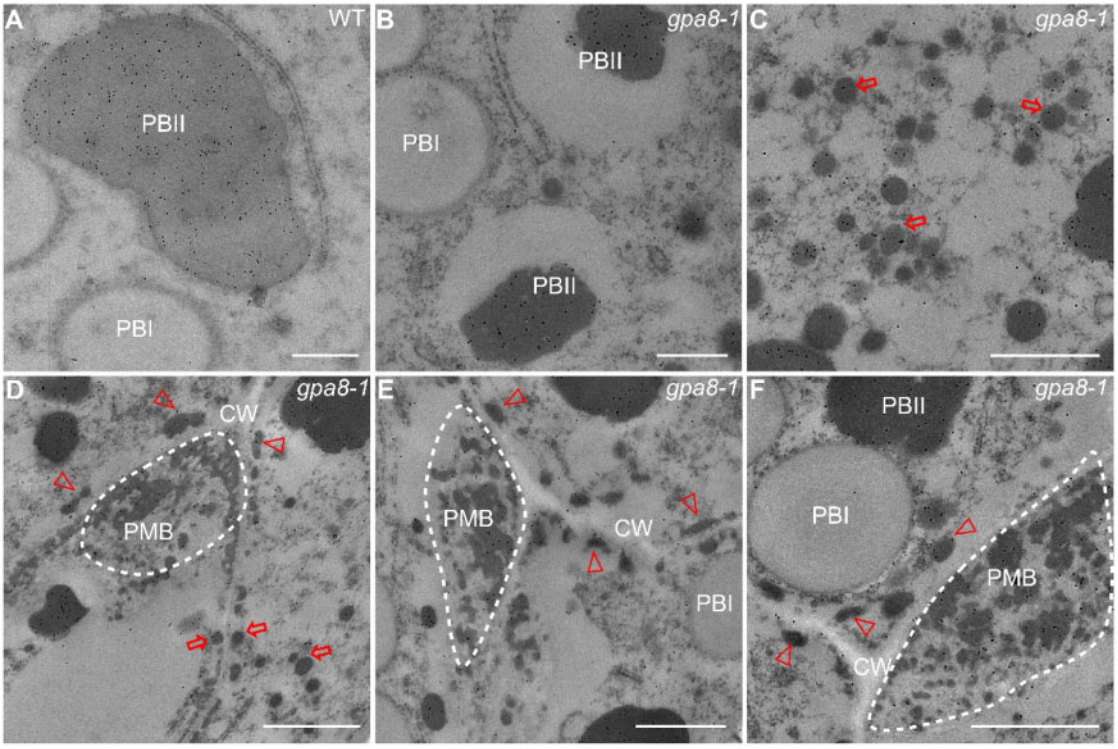

Figure 4 Immunoelectron microscopy localization of glutelins in rice endosperm cells. A, Glutelins accumulated in PBIIs in WT endosperm cells. Bars = 500 nm. B, PBIIs in the *gpa8-1* mutant were partially filled with glutelins. Bars = 500 nm. Irregular and round shape protein bodies indicate PBIIs and PBIs, respectively. C, Large clusters of DVs (red arrows) in the cytosol. Bars = 800 nm. D–F, Glutelins in DVs (red arrows), electron-dense granules (arrowheads), and PMB structures (dotted boxes) in *gpa8-1*. CW, cell walls. Bars = 1 μm in (D) and (F), Bars = 800 nm in (E). The 10-nm gold particle conjugated secondary antibodies were used in (A–F).

analysis revealed that *OsVHA-E1* was expressed in all tissues examined, including roots, leaves, leaf sheaths, stems, spikelets, and endosperm, with relatively higher expression in the roots and leaves. Expression of *OsVHA-E1* was high during early endosperm development and much lower at the late stages (Supplemental Figure S15). OsVHA-E2 is mainly expressed in panicles. *OsVHA-E3* was also expressed in all tissues examined. However, *OsVHA-E3* was much lower expressed than the *OsVHA-E1*.

To determine the subcellular localization of OsVHA-E1, the *OsVHA-E1* coding sequence was fused to the N-terminus of GFP to obtain a *p35S::OsVHA-E1-GFP* construct. Transformation into the *gpa8-1* mutant completely rescued the mutant phenotype, indicating that OsVHA-E1-GFP was functional in vivo (Supplemental Figure S16). We observed fluorescence signals of OsVHA-E1-GFP in protoplasts and root tip cells of *gpa8-1*-complemented plants. By colocalization analyses in protoplasts of *gpa8-1*-complemented plants, OsVHA-E1-GFP were localized to the TGN and tonoplast (Figure 6, A–H). In addition, our immunoelectron microscopy analysis using high pressure frozen/freeze substituted (HPF/FS) biological samples with anti-GFP antibodies further confirmed that OsVHA-E1-GFP were also localized to the TGN and tonoplast in root tip cells of *gpa8-1*-complemented plants (Figure 6, I–K).

We performed immunoprecipitation-mass spectrometry (IP-MS) using OsVHA-E1-GFP complemented transgenic lines to confirm that OsVHA-E1 is an integral part of the V-ATPase complex (Figure 7A). Most of the V-ATPase complex members were identified, including OsVHA-A1, OsVHA-A2, OsVHA-B1, OsVHA-B2, OsVHA-C, OsVHA-D, OsVHA-E1, OsVHA-E3, OsVHA-F, OsVHA-G, OsVHA-H1, OsVHA-H2, OsVHA-a1, OsVHA-a2, OsVHA-c, and OsVHA-d (Figure 7, A and B; Supplemental Table S3). We also measured the V-ATPase activity in 12 DAF endosperm of the WT and *gpa8-1* mutant. As expected, V-ATPase activity in the *gpa8-1* mutant was lower (Figure 7C). Together, these data indicated that OsVHA-E1 is indeed a functional component of the V-ATPase complex.

The luminal pH of TGN and the vacuole is increased in *gpa8-1* protoplasts

Previous studies showed that V-ATPase regulates the pH homeostasis of some cell organelles, such as TGN and vacuoles (Krebs et al., 2010; Luo et al., 2015). In order to determine whether cellular pH was affected in the *gpa8-1* mutant, we used live-cell imaging to measure pH of the TGN and vacuole by the pHluorin-based pH sensor and pH-sensitive fluorescent dye BCECF-AM (Krebs et al., 2010; Martinière et al., 2013; Shen et al., 2013). The pH sensor PRpHluorin-BP80 (Y612A) was used to measure the pH of TGN in rice protoplasts (Shen et al., 2013). The calibration curve was acquired by calculating pH-dependent fluorescence ratios (Figure 8A). Our results showed that the pH of TGN and the vacuole was increased in the *gpa8-1* mutant (TGN: 6.79 ± 0.19;

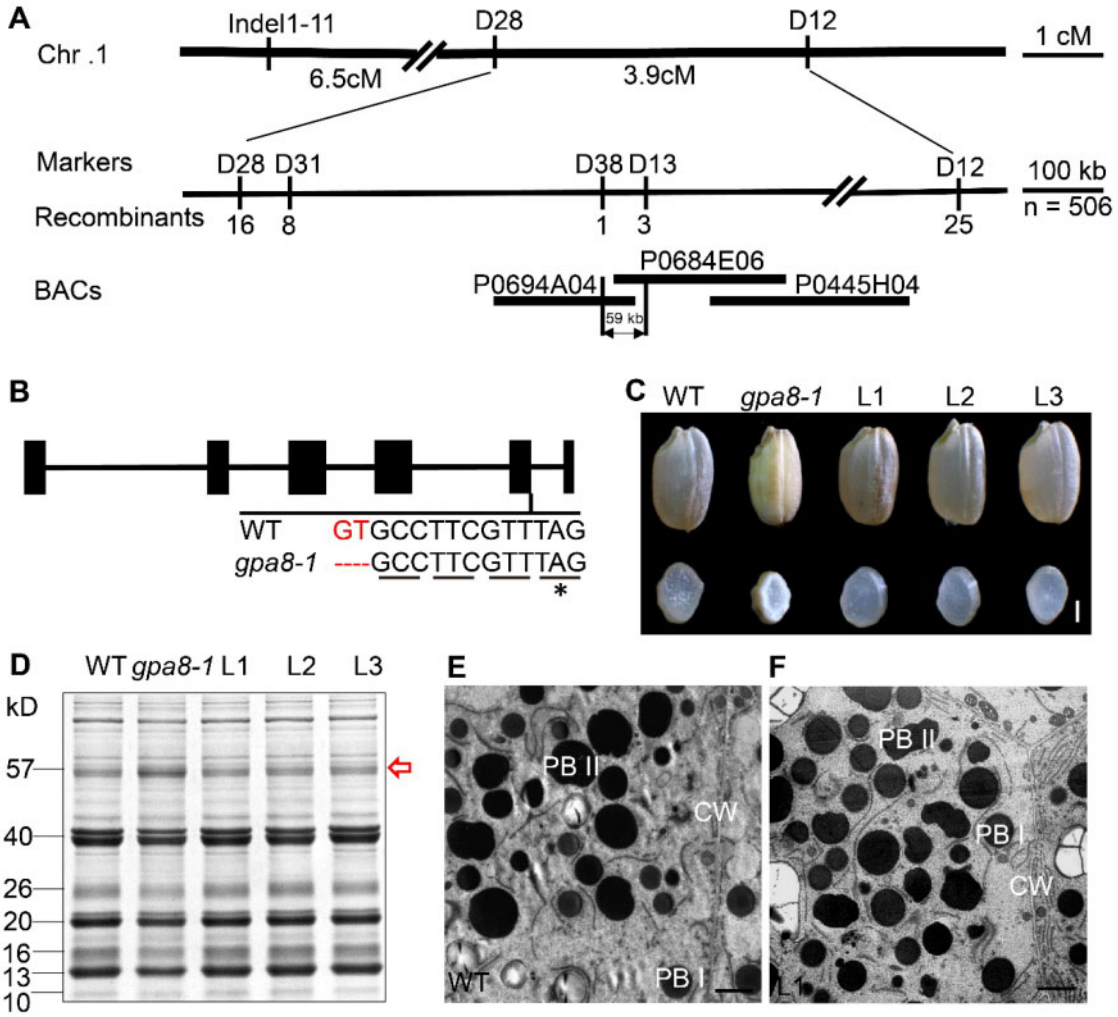

Figure 5 Map-based cloning of *GPA8*. A, Fine mapping of the *GPA8* locus. Molecular markers and numbers of recombinants are shown. B, Gene structure and the mutation site in *LOC_Os01g46980* comprising six exons (closed boxes) and five introns (lines). ATG and TGA represent the start and stop codons, respectively. C–F, *LOC_Os01g46980* coding sequence under the control of maize *ubiquitin* promoter rescues grain appearance (C), the storage protein composition pattern (D), the ultrastructures of endosperm cells in the WT (E), and L1 (F). Irregular and round shape protein bodies indicate PBIIs and PBIs, respectively. CW, cell wall. L1–L3 denote grains from three independent T_1 transgenic lines. Red arrow indicates the 57-kDa proglutelins. Bars = 1 mm in (C). Bars = 2 μm in (E) and (F).

vacuole: 6.36 ± 0.17) compared with the WT (TGN: 6.28 ± 0.15; vacuole: 5.72 ± 0.13; Figure 8, A–F). Representative pseudocolored images of PRpHluorin-BP80 (Y612A) are shown in Figure 8, B and C. These results indicated that OsVHA-E1 plays an important role in the pH homeostasis of the TGN and vacuole in rice protoplasts.

Subcellular localization of GPA1 and GPA3 are altered in *gpa8-1*

Previous studies showed that GPA1 and GPA3 regulate DV-mediated post-Golgi traffic in rice. GPA1 and GPA3 are partially localized to the TGN (Wang et al., 2010; Ren et al., 2014). As OsVHA-E1 regulates the pH homeostasis of the TGN, it is interesting to determine whether OsVHA-E1 is required for the localization of GPA1 and GPA3. We observed subcellular colocalization of GPA1 and GPA3 with mRFP-SYP61 (TGN marker) by transient expression in leaf protoplasts isolated from WT and *gpa8-1* (Wu et al., 2016; Lee et al., 2017). We found that although GFP-GPA1 and GPA3-GFP remain punctate patterns, they were less colocalized with mRFP-SYP61 in *gpa8-1* than in WT (Pearson's correlation coefficient [PSC], GPA1: PSC = 0.31 ± 0.06 [WT], PSC = 0.05 ± 0.02 [*gpa8-1*], GPA3: PSC = 0.28 ± 0.07 [WT], PSC = 0.04 ± 0.02 [*gpa8-1*]; Figure 9). When protoplasts were incubated in an acidic equilibration buffer at pH 6.2 (Reguera et al., 2015), the lowered colocalization in *gpa8-1* was recovered to the WT level (GPA1: PSC = 0.32 ± 0.06 [WT], PSC = 0.27 ± 0.09 [*gpa8-1*], GPA3: PSC = 0.25 ± 0.08 [WT], PSC = 0.21 ± 0.09 [*gpa8-1*]; Supplemental Figure S17). Together, the endosomal pH value is essential for proper protein localization, such as GPA1 and GPA3. The altered localization of both proteins might lead to post-Golgi trafficking defects in *gpa8-1*.

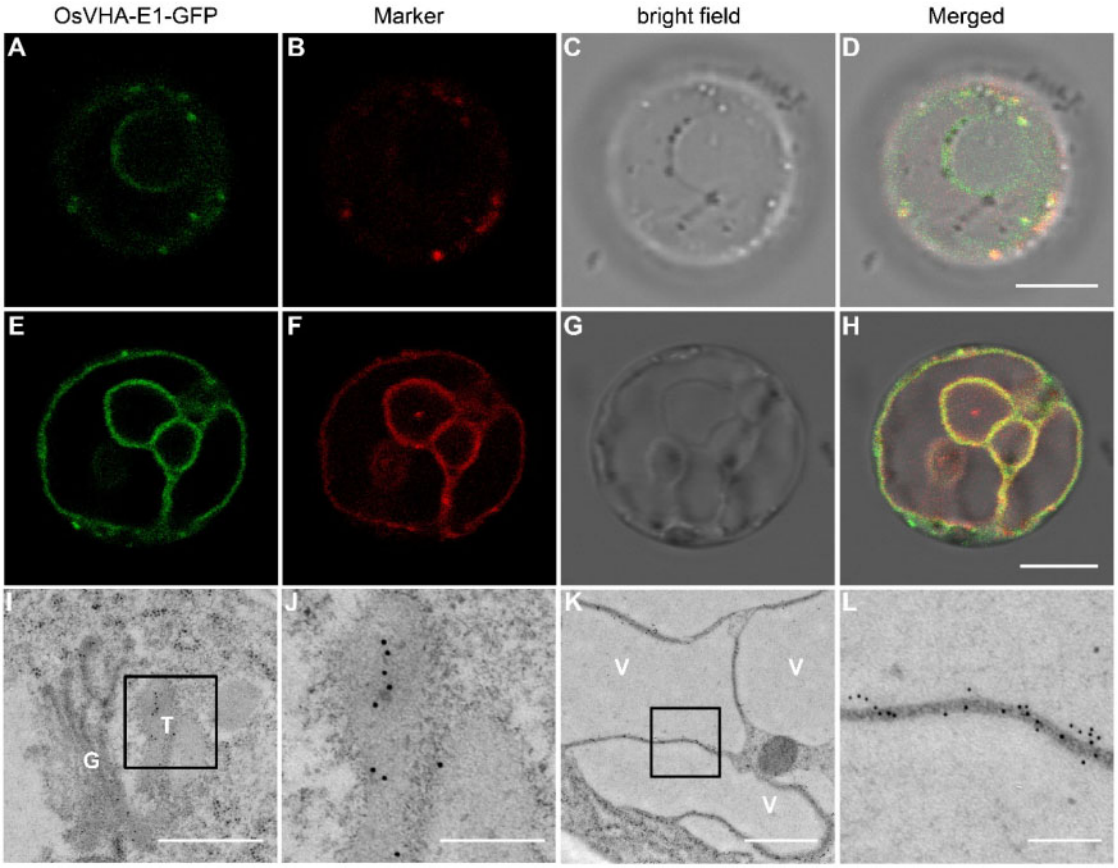

Figure 6 Subcellular localization of OsVHA-E1. A–H, Subcellular localization of OsVHA-E1 in protoplasts of *gpa8-1*-complemented plants. OsVHA-E1-GFP were localized to the TGN and tonoplast. I–L, Subcellular localization of OsVHA-E1 in root tip cells of *gpa8-1*-complemented plants. Sections were prepared by the HPF/FS method. Immunoelectron microscopy analysis with anti-GFP antibodies revealed that OsVHA-E1-GFP were also localized to the TGN and tonoplast. Bars = 8 μm in (A–H). Bars = 600 nm in (I), 200 nm in (J, L), and 800 nm in (K). G, Golgi, T, TGN, V, vacuole. The 10-nm gold particle conjugated secondary antibodies were used in (I–L).

OsVHA-E1 is essential for post-Golgi transport pathways

In order to determine whether V-ATPase is involved in the secretory and vacuolar trafficking of other proteins in rice, we chose two marker proteins (tonoplast: AtVIT1; plasma membrane: OsSCAMP1) and observed their subcellular localization in protoplasts (Kim et al., 2006; Lam et al., 2007). AtVIT1 and OsSCAMP1 in the WT were correctly localized to the tonoplast and plasma membrane, respectively (Figure 10, A and C). However, in the *gpa8-1* mutant, they exhibited incorrect cytoplasmic localizations and were not targeted to the tonoplast or plasma membrane (Figure 10, B and D). In order to determine whether V-ATPase was involved in endocytic trafficking we used the endocytotic tracer FM4-64 (Ueda et al., 2001). Within 20 min, FM4-64 labeled both plasma membranes of WT and *gpa8-1* root tip cells (Figure 10E). Then FM4-64 did not differentially label the endosomes/TGN after treatment for 90 min in both WT and *gpa8-1* (Figure 10F). However, after treatment for 180 min, FM4-64 reached the vacuolar membrane in WT, but remained in punctate structures in the *gpa8-1* mutant (Figure 10G). This indicated that endocytic trafficking from the TGN to vacuoles was delayed in the mutant. Therefore, these results suggested that OsVHA-E1 functions in post-Golgi transport pathways in rice.

Discussion

gpa8 is defective in post-Golgi trafficking of storage proteins in rice endosperm cells

Characterization of 57H mutants facilitated an understanding of the molecular mechanism of proglutelin trafficking and processing in rice endosperm cells. In this study, we isolated a 57H mutant *gpa8-1* that accumulated large amounts of proglutelins in rice endosperm. Similar protein levels of BiP1 and PDI1-1 in WT and the *gpa8-1* mutant suggested a normal ER function in the mutant (Figure 1F). The mutant also developed normal ER-derived PBIs. Differing from previously reported 57H (*gpa*) mutants defective in post-Golgi trafficking (Takemoto et al., 2002; Wang et al., 2009, 2010; Fukuda et al., 2011, 2013; Liu et al., 2013; Ren et al., 2014, 2020; Zhu et al., 2019) the *gpa8-1* mutant formed bent Golgi stacks, reduced TGN bodies, and enlarged DVs (Figure 3, C and D). Numerous DVs varying in size and electron density aggregated around the Golgi apparatus to form large clusters (Figure 3, E and F). The smaller DVs with lower electron density seemed to be immature. All these features suggested that DV biogenesis was delayed in the *gpa8-1* mutant. Finally, some DVs were missorted to the apoplast forming complex PMBs, leading to smaller PBIIs in the *gpa8-1*

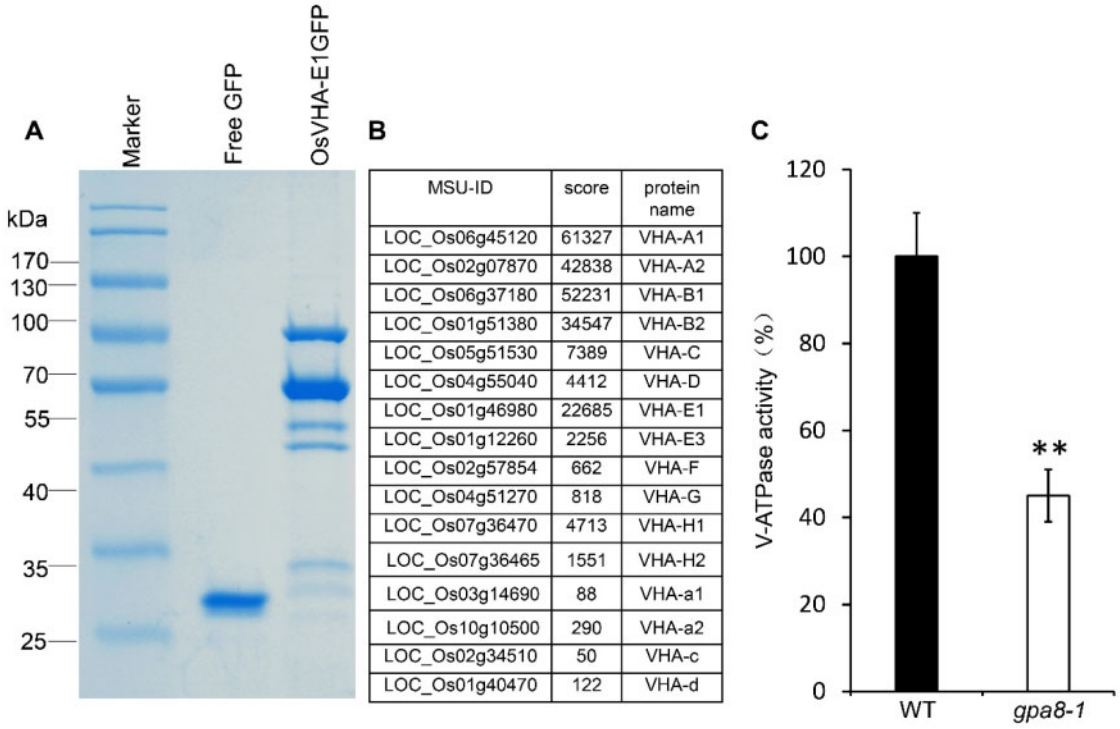

MSU-ID	score	protein name
LOC_Os06g45120	61327	VHA-A1
LOC_Os02g07870	42838	VHA-A2
LOC_Os06g37180	52231	VHA-B1
LOC_Os01g51380	34547	VHA-B2
LOC_Os05g51530	7389	VHA-C
LOC_Os04g55040	4412	VHA-D
LOC_Os01g46980	22685	VHA-E1
LOC_Os01g12260	2256	VHA-E3
LOC_Os02g57854	662	VHA-F
LOC_Os04g51270	818	VHA-G
LOC_Os07g36470	4713	VHA-H1
LOC_Os07g36465	1551	VHA-H2
LOC_Os03g14690	88	VHA-a1
LOC_Os10g10500	290	VHA-a2
LOC_Os02g34510	50	VHA-c
LOC_Os01g40470	122	VHA-d

Figure 7 *GPA8* encodes a functional subunit E1 of vacuolar H^+-ATPase. A and B, Mass spectrometry analysis of the rice V-ATPase complexes. A, Coomassie brilliant blue-stained SDS–PAGE of *p35S::GFP* transgene (left lane) and *p35S::OsVHA–GFP* transgene immunoprecipitates (right lane). B, Some OsVHA-E1-interacting proteins identified by mass spectrometry analysis. C, V-ATPase activity. Three biological replicates were performed, values are means ± SD. $^{**}P < 0.01$; Student's *t* test.

mutant as in other 57H mutants (Figure 3, H–L). Taken together, the *gpa8-1* mutant is defective in DV biogenesis and the subsequent DV-mediated proglutelin post-Golgi vacuolar trafficking pathway in endosperm cells.

GPA8 encodes subunit E1 of V-ATPase and is homologous to *AtVHA-E1*. In Arabidopsis, V-ATPases are localized to the TGN and tonoplast that are marked by different localization isoforms (VHA-a1: TGN; VHA-a2 and VHA-a3: tonoplast; Dettmer et al., 2006). AtVHA-E1 was also localized to the TGN and tonoplast by immunoelectron microscopy (Strompen et al., 2005; Dettmer et al., 2006). OsVHA-E1-GFP were also localized to the TGN and tonoplast in protoplasts and root tip cells of *gpa8-1*-complemented plants (Figure 6). In Arabidopsis, knockout mutant of subunit E isoform 1 (*tuff/atvha-E1*) is embryonic lethal, exhibiting horseshoe-shaped Golgi stacks, large vacuoles, and cells with multiple nuclei and abnormal cell wall deposition (Strompen et al., 2005). The homozygous *gpa8-1* mutant is a knockdown mutant of OsVHA-E1. Bent Golgi stacks were similar in *tuff* embryos and *gpa8-1* endosperm cells. However, DV budding and subsequent DV-mediated proglutelin post-Golgi vacuolar trafficking pathways were defective in the *gpa8-1* mutant.

pH homeostasis of endomembrane compartments is important for vacuolar transport pathway in rice

Intracellular pH is regulated by the activity of H^+ pumps and the H^+-leak pathway (Paroutis et al., 2004; Schumacher, 2014). Pumps including the plasma membrane P-type H^+-ATPase, V-ATPase, and H^+-pyrophosphatase have been extensively reported. The H^+-leak pathway including NHX-type Na^+/H^+ antiporters is responsible for alkalinizing mechanisms of pH homeostasis. Like animals, plant cells also have specific pH levels in different endomembrane compartments along the secretory pathway (ER: pH 7.1; Golgi: pH 6.8; TGN: pH 6.3; PVC: pH 6.2; vacuole: pH 5.9 in Arabidopsis; Shen et al., 2013). In this study, we found that the pH values of TGN and vacuole in WT rice protoplasts were similar to their counterparts in Arabidopsis protoplasts. However, TGN and the vacuole had a higher pH (TGN: ΔpH = 0.51; vacuole: ΔpH = 0.64) in *gpa8-1* (Figure 8), indicating that OsVHA-E1 plays an important role in acidification of these compartments.

The precise regulation of intracellular pH is indispensable to various biological processes in all organisms, such as protein sorting, enzyme activity, endocytosis, receptor–cargo interaction, and posttranslational modifications or processing of secreted proteins (Paroutis et al., 2004). The membrane trafficking pathways comprise three major types: the biosynthetic–secretory pathway, the endocytic pathway, and the vacuolar transport pathway (Uemura and Ueda, 2014). Previous studies implicated that acidification of TGN by V-ATPase was required for endocytic and secretory trafficking in Arabidopsis (Dettmer et al., 2006; Luo et al., 2015). However, whether V-ATPases are involved in the vacuolar transport pathway is unclear. In addition, alkalization of

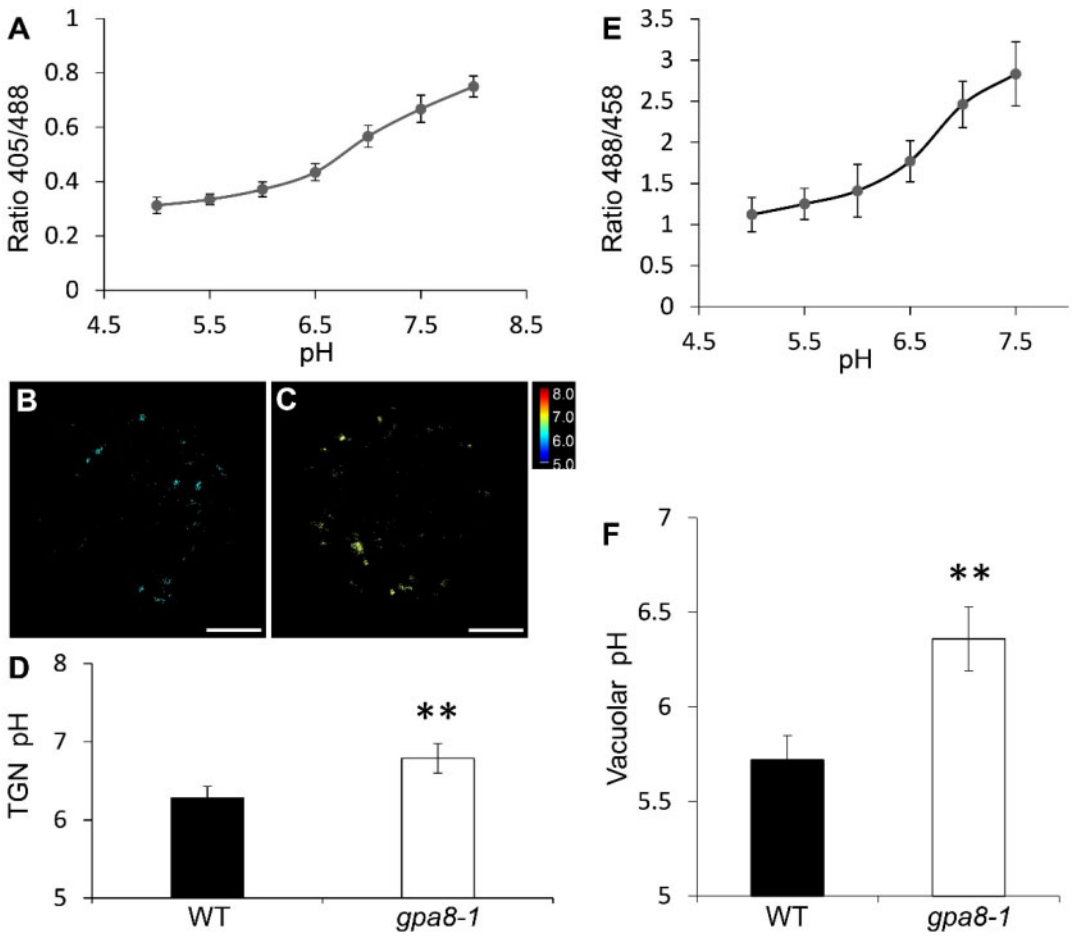

Figure 8 OsVHA-E1 regulates pH of TGN and vacuole. A, In vivo calibration curve of pH. pH calibration was achieved by equilibrating intracellular pH with 10 μM nigericin, 60-mM KCl, and 10-mM MES/HEPES Bis–Tris–propane, pH 5.0–8.0 (means ± SD; $n \geqslant 25$ protoplasts). B and C, Representative pseudocolored images of PRpHluorin-BP80 (Y612A) in WT (B) and *gpa8-1* (C) protoplasts. Bars = 5 μm. D, pH of the TGN (means ± SD; $n \geqslant 25$ protoplasts; $^{**}P < 0.01$; Student's *t* test). E, In vivo calibration curve of pH of BCECF-AM dye. pH equilibration buffers contain 50-mM Mes-BTP (pH 5.0–6.5) or 50-mM HEPES-BTP (pH 7.0–7.5) and 50-mM ammonium acetate (means ± SD; $n \geqslant 15$ roots). F, Vacuolar pH (means ± SD; $n \geqslant 15$ roots; $^{**}P < 0.01$; Student's *t* test).

endomembrane compartments by AtNHX5/6 and OsNHX5 is required for protein trafficking to the vacuole in Arabidopsis and rice (Reguera et al., 2015; Zhu et al., 2019). In an *atnhx5 atnhx6* double mutant, a lowered pH led to a compromised receptor–cargo association. Considering that storage proteins were missorted to apoplasts in *osvha-E1* and *atnhx5 atnhx6*, the altered pH of TGN might result in reduced VSR–proglutelin association, although the receptors for proglutelins remain to be characterized. The altered pH influences the recruitment of the small GTPase Arf6 and ARNO from cytosol to endosomal membranes in animal cells (Maranda et al., 2001; Hurtado-Lorenzo et al., 2006). We found that GFP-GPA1 and GPA3-GFP were less colocalized with mRFP-SYP61 in *gpa8-1* (Figure 9). The colocalization was recovered when protoplasts were incubated in an acidic equilibration buffer. These results suggested that the subcellular localization of GPA1 and GPA3 is pH dependent (Supplemental Figure S17). DVs are unique carriers for proglutelin transport in rice presumably budded from the TGN (Liu et al., 2013; Ren et al., 2014). The changed subcellular localization of GPA1 and GPA3 might affect post-Golgi trafficking efficiency of DVs in *gpa8-1*. The average size of DVs newly budded from TGN is enlarged to about 295 nm in *gpa8-1*, which is much bigger than 157 nm in the WT. Therefore, pH of TGN may influence biogenesis of DVs in rice, although the detailed mechanism remains to be further explored. In addition, the altered pH of the TGN in the *gpa8-1* mutant had an impact on other proteins of post-Golgi transport pathways in rice, such as AtVIT1 and OsSCAMP1 (Figure 10, A–D). An FM4-64 staining experiment also showed that OsVHA-E1 was involved in the endocytic trafficking pathway (Figure 10, E–G). Notably, IP-MS analysis showed that OsVHA-E1 together with some actin filaments and tubulins might form a complex in vivo, indicating that the bent Golgi in the *gpa8-1* mutant was related to actin filaments and tubulins (Supplemental Table S3; Ma et al., 2012).

The *gpa8-1* mutant exhibited a lesion-mimic phenotype similar to the leaf tip necrosis observed for *atvha-a2 atvha-*

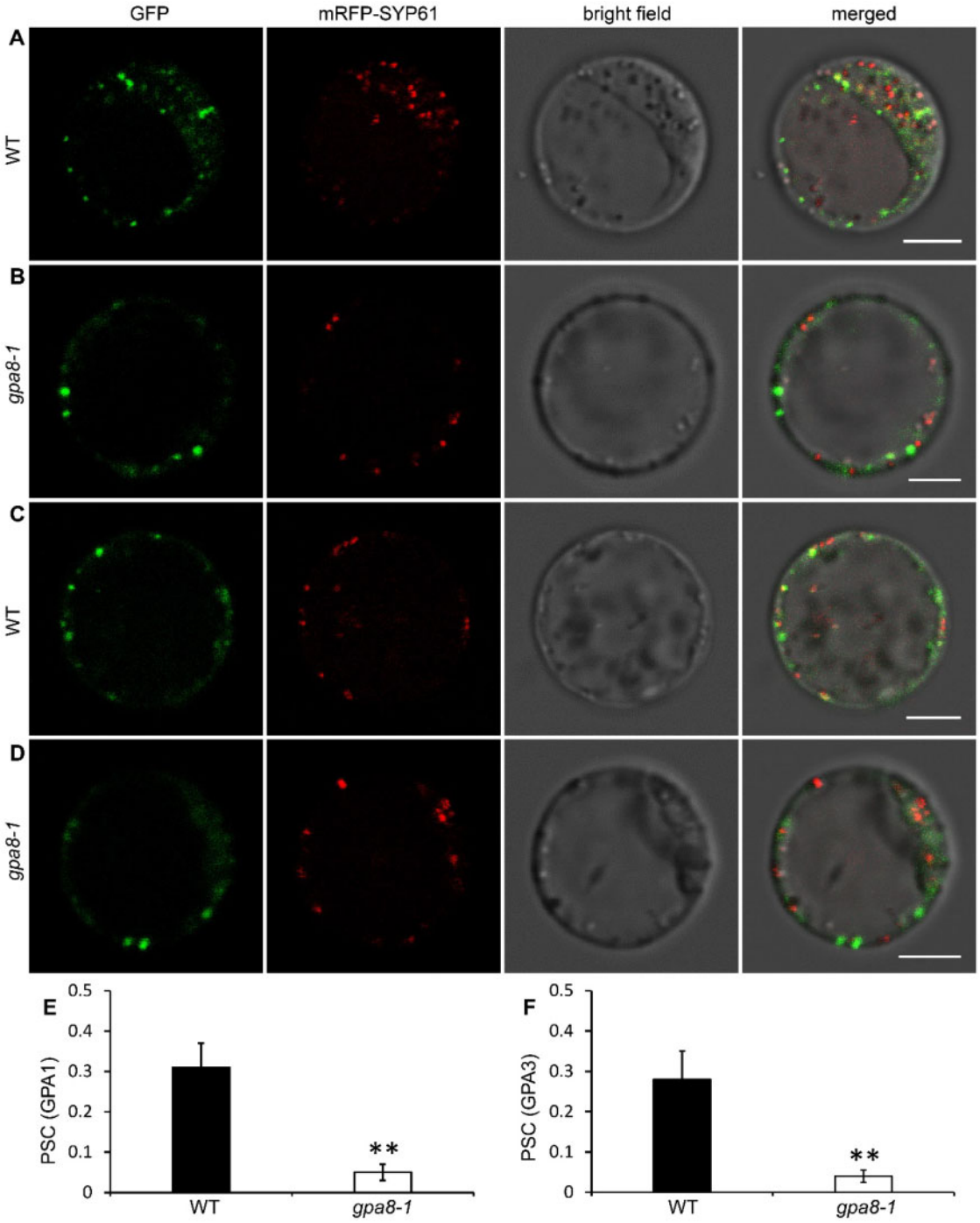

Figure 9 Subcellular localization of GPA1 and GPA3 are altered in *gpa8-1*. A and B, Localization of GFP-GPA1 in WT (A) and *gpa8-1* (B) protoplasts. C and D, Localization of GPA3-GFP in WT (C) and *gpa8-1* (D) protoplasts. mRFP-SYP61 serves as a TGN marker. Bars = 5 μm in (A–D). E and F, PSC of GPA1 (E) and GPA3 (F) with mRFP-SYP61. Values are means ± SD. $^{**}P < 0.01$ (n = 45 protoplasts, Student's t test).

a3 (Krebs et al., 2010). As AtVHA-a2 and AtVHA-a3 are localized to the tonoplast, the increased vacuolar pH might be connected with the lesion-mimic phenotype (Supplemental Figure S1), although the detailed mechanism needs to be determined.

In summary, our studies demonstrated that OsVHA-E1 maintains Golgi and TGN morphology as well as pH homeostasis of TGN, a requirement for DV biogenesis and subsequent protein trafficking in rice endosperm.

Materials and methods

Plant materials and growth conditions

The rice (*O. sativa*) *gpa8-1* and *gpa8-2* mutants were generated by MNU treatment of *japonica* variety Ninggeng 1. All plants were grown in paddy fields during the normal growing seasons or in a greenhouse at Nanjing, China. Developing seeds of the WT (Ninggeng 1) and *gpa8-1* mutant at 6–21 DAF were used in the experiments.

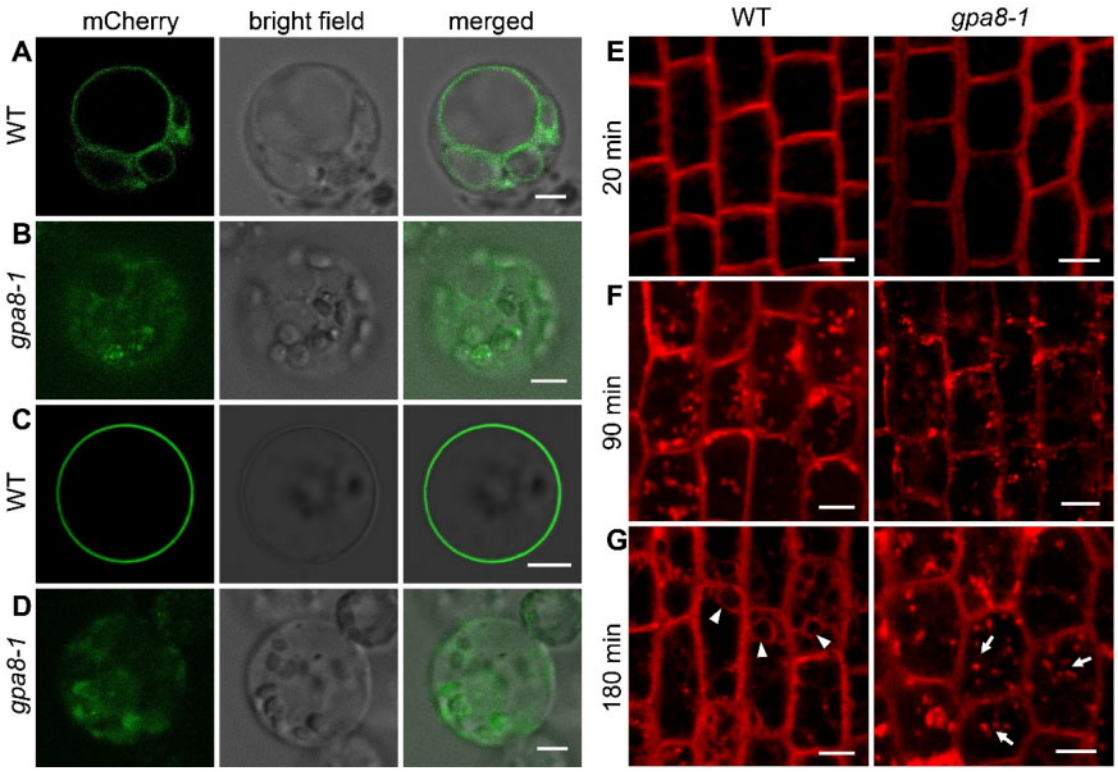

Figure 10 OsVHA-E1 is critical for protein sorting in the post-Golgi trafficking pathway. A and B, Localization of mCherry-VIT1 in WT (A) and *gpa8-1* (B) protoplasts. C and D, Localization of SCAMP1-mCherry in WT (C) and *gpa8-1* (D) protoplasts. Bars = 5 μm in (A–D). E–G, Roots of WT and *gpa8-1* seedlings were stained with FM4-64. Root tip cells were observed at 20 min (E), 90 min (F), and 180 min (G) after staining. Bars = 10 μm in (E–G). Arrowheads represent vacuolar membranes and arrows indicate FM4-64 labeled endosomes.

Measurement of starch and total protein contents

Rice grains were processed in a drying oven and ground into fine flour with a miller. Amylose and total protein contents were subsequently measured according to previous report (Han et al., 2012).

Protein extraction from rice seeds and immunoblot analysis

Total protein extraction and immunoblot assay were performed as described previously (Wang et al., 2016).

Microscopy

Scanning electron microscopy, TEM, light, and immunofluorescence microscopy were performed as described previously (Wang et al., 2010; Liu et al., 2013; Ren et al., 2014).

For immunogold electron microscopy, root tips of 5-d-old seedlings were HPF/FS, followed by ultrasection and immunogold labeling as described previously (Ren et al., 2014, 2020). Briefly, root tips of *gpa8-1*-complemented seedlings were fixed by high-pressure freezing (EMPACT2, Leica) and freeze substituted with 0.2% (w/v) uranyl acetate in acetone at −85°C for 24 h, followed by a series of gradient dehydration. The samples were embedded in LOWICRYL HM20 resin after dehydration. Ultrathin sections (70 nm in thickness) were acquired using an EM UC7 microtome (Leica). Immunogold labeling sections were obtained with anti-GFP antibodies. The 10-nm gold particle conjugated secondary antibodies were used.

Map-based cloning

An F_2 population was generated from a cross between the *gpa8-1* mutant and an *indica* variety N22 to map the *GPA8* locus. Total proteins were extracted from the distal halves of individual rice seeds and subjected to SDS–PAGE to monitor the accumulation of the proglutelins. The other halves of identified mutant seeds were grown for DNA extraction. A total of 506 individuals with the recessive phenotype were used for fine mapping of *GPA8*. The primers used in fine mapping are listed in Supplemental Table S4.

RT-qPCR analysis

Total RNA was extracted from various tissues using an RNA Prep Pure Plant Kit (TIANGEN). First strand cDNA was synthesized using oligo(dT)18 as the primer (TaKaRa, Japan). Three biological replicates of RT-qPCR were performed with SYBR Premix Ex Taq II (TaKaRa) on an Applied Biosystems 7500 Real-Time PCR System. The primer sequences used for PCR are listed in Supplemental Table S5.

Subcellular localization

To determine the subcellular localization of OsVHA-E1, rice protoplasts were isolated from OsVHA-E1-GFP transgenically complemented seedlings (Chen et al., 2006; Supplemental

Table S6). To determine the subcellular localization of GFP-GPA1, GPA3-GFP, mCherry-VIT1, and SCAMP1-mCherry, the protoplasts were isolated from 10-d-old WT and *gpa8-1* mutant seedlings. *gpa8-1* protoplasts were incubated for 5 min in acidic equilibration buffer, pH 6.2. pH was equilibrated with 10-μM nigericin, 60-mM KCl, and 10-mM MES/HEPES Bis–Tris–propane. The transient expression constructs were separately transformed into rice protoplasts and incubated in darkness at 28°C for 16 h prior to examination (Chen et al., 2006). Fluorescence was observed using a confocal laser scanning microscope (Leica TCS-SP8). GFP signals with white light laser at emission wavelength of 505–530 nm were recorded with the excitation wavelength at 488 nm, mCherry signals with white light laser at emission wavelength of 600–630 nm were recorded with the excitation wavelength at 587 nm.

Immunoprecipitation and mass spectrometry

Two-week-old OsVHA-E1-GFP T1 transgenically complemented seedlings or GFP transgenic seedlings were pulverized in liquid nitrogen and NB1 buffer (50-mM Tris-MES, pH 8.0, 0.5-M sucrose, 1-mM $MgCl_2$, 10-mM EDTA, 5-mM DTT, 20-mM NaF, and complete proteinase inhibitors) and centrifuged at 12,000*g* for 30 min at 4°C. Extracts were incubated with anti-GFP-agarose beads for 2 h and centrifuged at 500*g* for 2 min at 4°C. The agarose beads were washed three times with NB1 buffer; then boiled in the 5× loading buffer for SDS–PAGE. The gels were excised for mass spectrometry.

Measurements of enzyme activity

Microsomal membrane proteins were extracted from WT and *gpa8-1* mutant endosperm at 12 DAF (Krebs et al., 2010). The V-ATPase (VHA) activity of 10 μg of microsomal membranes was obtained as a P_i release after 40 min of incubation at 28°C. A 10-μg bovine serum albumin was used as the negative control and reactions were terminated by using 40-mM citric acid. VHA activity assays were performed as described previously (Krebs et al., 2010; Zhang et al., 2013).

pH measurements in the TGN

Rice protoplasts were isolated from 10-d-old WT and *gpa8-1* seedlings. pH sensor PRpHluorin-BP80 (Y612A) was transformed into rice protoplasts as previously described (Chiu et al., 1996; Chen et al., 2006). Fluorescence images were acquired using a confocal laser scanning microscope (Leica TCS-SP8).

PRpHluorin signals at emission wavelength of 500–550 nm were recorded with the dual-excitation wavelength at 405 and 488 nm, respectively, and used to calculate the pH using the calibration curve. Ratio values were acquired using ImageJ. In vivo calibration was achieved from the same protoplasts expressing PRpHluorin for pH measurement. Protoplasts were incubated in WI buffer (0.5-M mannitol and 20-mM KCl) with 25 μM of nigericin, 60-mM KCl, and 10-mM MES/HEPES Bis–Tris–propane adjusted to pH values ranging from 5.0 to 8.0 for each calibration point (Martinière et al., 2013; Shen et al., 2013; Reguera et al., 2015; Fan et al., 2018).

Vacuolar pH measurement

Vacuolar pH of 4-d-old seedlings was measured using the pH-sensitive fluorescent dye BCECF-AM (Krebs et al., 2010). Seedlings were stained in liquid medium containing 1/10 murashige skoog (MS) medium, 0.5% w/v sucrose, 10-mM MES (pH 5.8), 10-μM BCECF-AM and 0.02% pluronic F-127 (Molecular Probes) for 1 h at 22°C in darkness. The seedlings were washed once for 10 min. BCECF-AM was excitated at 488 and 458 nm, and emission was detected between 530 and 550 nm, respectively. The ratio values were acquired using ImageJ. For pH calibration, seedlings were incubated in pH equilibration buffers containing 50-mM MES-BTP (pH 5.0–6.5) or 50-mM HEPES-BTP (pH 7.0–7.5) and 50-mM ammonium acetate for 15 min. Fluorescent images were acquired using a confocal laser scanning microscope (Leica TCS-SP8).

Accession numbers

Sequence data from this article can be found in the GenBank/EMBL databases under the following accession numbers: VHA-E1 (Os01g0659200), BiP1 (Os02g0115900), PDI1-1 (Os11g0199200), and TIP3 (Os10g0492600).

Supplemental data

The following materials are available in the online version of this article.

Supplemental Figure S1. Phenotypic characterization of wild type and *gpa8-1*.

Supplemental Figure S2. Relative intensities of protein bands in SDS-PAGE and immunoblotting assays.

Supplemental Figure S3. Time-course analysis of storage protein accumulation during endosperm development of wild-type Ninggeng 1 and the *gpa8-1* mutant.

Supplemental Figure S4. RT-qPCR assay of the expression of representative genes coding for storage proteins in 12 DAF endosperm.

Supplemental Figure S5. Light microscopy of protein bodies in subaleurone cells of wild-type and the *gpa8-1* mutant.

Supplemental Figure S6. Size of PBI in wild-type and the *gpa8-1* mutant.

Supplemental Figure S7. Size of PSV/PBII in wild-type and the *gpa8-1* mutant.

Supplemental Figure S8. Immunofluorescence microscopy of protein bodies in the sub-aleurone cells of wild-type and the *gpa8-1* mutant.

Supplemental Figure S9. Distribution of cell wall materials in 12 DAF endosperm cells.

Supplemental Figure S10. Distribution of Golgi stacks in 12 DAF endosperm cells.

Supplemental Figure S11. Genetic complementation.

Supplemental Figure S12. CRISPR/Cas9 lines of *OsVHA-E1*.

Supplemental Figure S13. Sequence and phylogenetic analyses of OsVHA-E1.

Supplemental Figure S14. Amino acid sequence alignment of OsVHA-E1 and its homologs.

Supplemental Figure S15. Spatial expression patterns of *OsVHA-E1*.

Supplemental Figure S16. Complementation of *gpa8-1* mutant phenotypes by *p35S::OsVHA-E1-GFP*.

Supplemental Figure S17. Intracellular acidification increased degree of colocalization of GPA1 and GPA3 with mRFP-SYP61 in *gpa8-1*.

Supplemental Table S1. Properties of wild type and *gpa8-1*.

Supplemental Table S2. Segregation of mutant phenotypes in reciprocal crosses between wild type and the *gpa8-1* mutant.

Supplemental Table S3. Mass spectrometry of OsVHA-E1-GFP immunoprecipitates.

Supplemental Table S4. Primers used for mapping.

Supplemental Table S5. Primers used for RT-qPCR analysis.

Supplemental Table S6. Primers used for vector construction.

Acknowledgments

We thank Prof. Liwen Jiang (School of Life Sciences, The Chinese University of Hong Kong) for pH sensors PRpHluorin-BP80 (Y612A), Prof. Quansheng Qiu, and Dr Ting Pan (School of Life Sciences, Lanzhou University) for help in pH measurements.

Funding

This research was supported by grants from National Key Research and Development Program of China (2016YFD0100501), National Natural Science Foundation of China (31830064 and 31671652), Jiangsu Agricultural Science and Technology Innovation Fund (CX(19)1002), Jiangsu Natural Science Foundation for Distinguished Young Scholars (BK20180024), Central Public-interest Scientific Institution Basal Research Fund (No. Y2020YJ09), and the Fundamental Research Funds for the Central Universities (KYTZ201601). This work was also supported by the Key Laboratory of Biology, Genetics, and Breeding of Japonica Rice in Mid-lower Yangtze River, Ministry of Agriculture, PR China, and the Jiangsu Collaborative Innovation Center for Modern Crop Production.

Conflict of interest statement. None declared.

References

Batelli G, Verslues PE, Agius F, Qiu Q, Fujii H, Pan S, Schumaker KS, Grillo S, Zhu JK (2007) SOS2 promotes salt tolerance in part by interacting with the vacuolar H^+-ATPase and upregulating its transport activity. Mol Cell Biol **27**: 7781–7790

Bechtel DR, Juliano BO (1980) Formation of protein bodies in the starchy endosperm of rice (*Oryza sativa* L.): a reinvestigation. Ann Bot **65**: 684–691

Chebli Y, Kaneda M, Zerzour R, Geitmann A (2012) The cell wall of the Arabidopsis pollen tube-spatial distribution, recycling, and network formation of polysaccharides. Plant Physiol **160**: 1940–1955

Chen SB, Tao LZ, Zeng LR, Vega-Sanchez ME, Umemura K, Wang GL (2006) A highly efficient transient protoplast system for analyzing defence gene expression and protein-protein interactions in rice. Mol Plant Pathol **7**: 417–427

Chiu WL, Niwa Y, Zeng W, Hirano T, Kobayashi H, Sheen J (1996) Engineered GFP as a vital reporter in plants. Curr Biol **6**: 325–330

Cui Y, Zhao Q, Gao CJ, Ding Y, Zeng YL, Ueda T, Nakano A, Jiang LW (2014) Activation of the Rab7 GTPase by the MON1-CCZ1 complex is essential for PVC-to-vacuole trafficking and plant growth in Arabidopsis. Plant Cell **26**: 2080–2097

Dettmer J, Hong-Hermesdorf A, Stierhof YD, Schumacher K (2006) Vacuolar H^+-ATPase activity is required for endocytic and secretory trafficking in Arabidopsis. Plant Cell **18**: 715–730

Dettmer J, Schubert D, Calvo-Weimar O, Stierhof YD, Schmidt R, Schumacher K (2005) Essential role of the V-ATPase in male gametophyte development. Plant J **41**: 117–124

Ebine K, Inoue T, Ito J, Ito E, Uemura T, Goh T, Abe H, Sato K, Nakano A, Ueda T (2014) Plant vacuolar trafficking occurs through distinctly regulated pathways. Curr Biol **24**: 1375–1382

Fan LG, Zhao L, Hu W, Li WN, Novak O, Strnad M, Simon S, Friml J, Shen JB, Jiang LW, Qiu QS (2018) Na^+, K^+/H^+ antiporters regulate the pH of endoplasmic reticulum and auxin-mediated development. Plant Cell Environ **41**: 850–864

Fuji K, Shirakawa M, Shimono Y, Kunieda T, Fukao Y, Koumoto Y, Takahashi H, Hara-Nishimura I, Shimada T (2016) The adaptor complex AP-4 regulates vacuolar protein sorting at the *trans*-Golgi network by interacting with VACUOLAR SORTING RECEPTOR1. Plant Physiol **170**: 211–219

Fukuda M, Satoh-Cruz M, Wen L, Crofts AJ, Sugino A, Washida H, Okita TW, Ogawa M, Kawagoe Y, Maeshima M et al. (2011) The small GTPase Rab5a is essential for intracellular transport of proglutelin from the Golgi apparatus to the protein storage vacuole and endosomal membrane organization in developing rice endosperm. Plant Physiol **157**: 632–644

Fukuda M, Wen L, Satoh-Cruz M, Kawagoe Y, Nagamura Y, Okita TW, Washida H, Sugino A, Ishino S, Ishino Y et al. (2013) A guanine nucleotide exchange factor for Rab5 proteins is essential for intracellular transport of the proglutelin from the Golgi apparatus to the protein storage vacuole in rice endosperm. Plant Physiol **162**: 663–674

Han XH, Wang YH, Liu X, Jiang L, Ren YL, Liu F, Peng C, Li JJ, Jin XM, Wu FQ et al. (2012) The failure to express a protein disulphide isomerase-like protein results in a floury endosperm and an endoplasmic reticulum stress response in rice. J Exp Bot **63**: 121–130

Hillmer S, Movafeghi A, Robinson DG, Hinz G (2001) Vacuolar storage proteins are sorted in the *cis*-cisternae of the pea cotyledon Golgi apparatus. J Cell Biol **152**: 41–50

Hinz G, Colanesi S, Hillmer S, Rogers JC, Robinson DG (2007) Localization of vacuolar transport receptors and cargo proteins in the golgi apparatus of developing Arabidopsis embryos. Traffic **8**: 1452–1464

Hinz G, Hillmer S, Baumer M, Hohl I (1999) Vacuolar storage proteins and the putative vacuolar sorting receptor BP-80 exit the Golgi apparatus of developing pea cotyledons in different transport vesicles. Plant Cell **11**: 1509–1524

Hohl I, Robinson DG, Chrispeels MJ, Hinz G (1996) Transport of storage proteins to the vacuole is mediated by vesicles without a clathrin coat. J Cell Sci **109**: 2539–2550

Hurtado-Lorenzo A, Skinner M, El Annan J, Futai M, Sun-Wada GH, Bourgoin S, Casanova J, Wildeman A, Bechoua S, Ausiello DA et al. (2006) V-ATPase interacts with ARNO and Arf6 in early endosomes and regulates the protein degradative pathway. Nat Cell Biol **8**: 124–U128

Kaida R, Hayashi T, Kaneko TS (2008) Purple acid phosphatase in the walls of tobacco cells. Phytochemistry **69**: 2546–2551

Kim SA, Punshon T, Lanzirotti A, Li LT, Alonso JM, Ecker JR, Kaplan J, Guerinot ML (2006) Localization of iron in Arabidopsis seed requires the vacuolar membrane transporter VIT1. Science **314**: 1295–1298

Krebs M, Beyhl D, Gorlich E, Al-Rasheid KAS, Marten I, Stierhof YD, Hedrich R, Schumacher K (2010) Arabidopsis V-ATPase activity at the tonoplast is required for efficient nutrient storage but not for sodium accumulation. Proc Natl Acad Sci USA **107**: 3251–3256

Krishnan HB, Franceschi VR, Okita TW (1986) Immunochemical studies on the role of the Golgi complex in protein-body formation in rice seeds. Planta **169**: 471–480

Kumamaru T, Uemura Y, Inoue Y, Takemoto Y, Siddiqui SU, Ogawa M, Hara-Nishimura I, Satoh H (2010) Vacuolar processing enzyme plays an essential role in the crystalline structure of glutelin in rice seed. Plant Cell Physiol **51**: 38–46

Lam SK, Siu CL, Hillmer S, Jang S, An GH, Robinson DG, Jiang LW (2007) Rice SCAMP1 defines clathrin-coated, *trans*-Golgi-located tubular-vesicular structures as an early endosome in tobacco BY-2 cells. Plant Cell **19**: 296–319

Lee MH, Yoo YJ, Kim DH, Hanh NH, Kwon Y, Hwang I (2017) The prenylated Rab GTPase receptor PRA1.F4 contributes to protein exit from the Golgi apparatus. Plant Physiol **174**: 1576–1594

Liu F, Ren YL, Wang YH, Peng C, Zhou KN, Lv J, Guo XP, Zhang X, Zhong MS, Zhao SL, et al. (2013) OsVPS9A functions cooperatively with OsRAB5A to regulate post-Golgi dense vesicle-mediated storage protein trafficking to the protein storage vacuole in rice endosperm cells. Mol Plant **6**: 1918–1932

Luo Y, Scholl S, Doering A, Zhang Y, Irani NG, Di Rubbo S, Neumetzler L, Krishnamoorthy P, Van Houtte I, Mylle E, et al. (2015) V-ATPase activity in the TGN/EE is required for exocytosis and recycling in Arabidopsis. Nat Plants **1**: 15094

Ma BY, Qian D, Nan Q, Tan C, An LZ, Xiang Y (2012) Arabidopsis vacuolar H^+-ATPase (V-ATPase) B subunits are involved in actin cytoskeleton remodeling via binding to, bundling, and stabilizing F-actin. J Biol Chem **287**: 19008–19017

Maranda B, Brown D, Bourgoin S, Casanova JE, Vinay P, Ausiello DA, Marshansky V (2001) Intra-endosomal pH-sensitive recruitment of the Arf-nucleotide exchange factor ARNO and Arf6 from cytoplasm to proximal tubule endosomes. J Biol Chem **276**: 18540–18550

Martinière A, Bassil E, Jublanc E, Alcon C, Reguera M, Sentenac H, Blumwald E, Paris N (2013) In *vivo* intracellular pH measurements in tobacco and Arabidopsis reveal an unexpected pH gradient in the endomembrane system. Plant Cell **25**: 4028–4043

Nishi T, Forgac M (2002) The vacuolar (H^+)-atpases—nature's most versatile proton pumps. Nat Rev Mol Cell Biol **3**: 94–103

Ogawa M, Kumamaru T, Satoh H, Iwata N, Takeshi O, Zenzaburo K, Kunisuke T (1987) Purification of protein body-I of rice seed and its polypeptide composition. Plant Cell Physiol **28**: 1517–1527

Otegui MS, Herder R, Schulze J, Jung R, Staehelin LA (2006) The proteolytic processing of seed storage proteins in Arabidopsis embryo cells starts in the multivesicular bodies. Plant Cell **18**: 2567–2581

Padmanaban S, Lin XY, Perera I, Kawamura Y, Sze H (2004) Differential expression of vacuolar H^+-ATPase subunit c genes in tissues active in membrane trafficking and their roles in plant growth as revealed by RNAi. Plant Physiol **134**: 1514–1526

Paroutis P, Touret N, Grinstein S (2004) The pH of the secretory pathway: Measurement, determinants, and regulation. Physiology **19**: 207–215

Pernollet JC, Mossé J (1983) Structural and location of legume and cereal seed storage proteins. *In* J Daussant, J Moss6, J Vaughan, eds, Seed Protein. Academic Press, London, New York, pp 155–191

Reguera M, Bassil E, Tajima H, Wimmer M, Chanoca A, Otegui MS, Paris N, Blumwald E (2015) pH regulation by NHX-type antiporters is required for receptor-mediated protein trafficking to the vacuole in Arabidopsis. Plant Cell **27**: 1200–1217

Ren YL, Wang YH, Liu F, Zhou KN, Ding Y, Zhou F, Wang Y, Liu K, Gan L, Ma WW, et al. (2014) GLUTELIN PRECURSOR ACCUMULATION3 encodes a regulator of post-Golgi vesicular traffic essential for vacuolar protein sorting in rice endosperm. Plant Cell **26**: 410–425

Ren YL, Wang YH, Pan T, Wang YL, Wang YF, Gan L, Wei ZY, Wang F, Wu MM, Jing RN, et al. (2020) GPA5 encodes a Rab5a effector required for post-Golgi trafficking of rice storage proteins. Plant Cell **32**: 758–777

Schumacher K (2014) pH in the plant endomembrane system - an import and export business. Curr Opin Plant Biol **22**: 71–76

Schumacher K, Krebs M (2010) The V-ATPase: small cargo, large effects. Curr Opin Plant Biol **13**: 724–730

Schumacher K, Vafeados D, McCarthy M, Sze H, Wilkins T, Chory J (1999) The Arabidopsis *det3* mutant reveals a central role for the vacuolar H^+-ATPase in plant growth and development. Genes Dev **13**: 3259–3270

Shen JB, Zeng YL, Zhuang XH, Sun L, Yao XQ, Pimpl P, Jiang LW (2013) Organelle pH in the Arabidopsis endomembrane system. Mol Plant **6**: 1419–1437

Shen Y, Wang JQ, Ding Y, Lo SW, Gouzerh G, Neuhaus JM, Jiang LW (2011) The rice RMR1 associates with a distinct prevacuolar compartment for the protein storage vacuole pathway. Mol Plant **4**: 854–868

Shimada T, Fuji K, Tamura K, Kondo M, Nishimura M, Hara-Nishimura I (2003) Vacuolar sorting receptor for seed storage proteins in Arabidopsis thaliana. Proc Natl Acad Sci USA **100**: 16095–16100

Strompen G, Dettmer J, Stierhof YD, Schumacher K, Jurgens G, Mayer U (2005) Arabidopsis vacuolar H^+-ATPase subunit E isoform 1 is required for Golgi organization and vacuole function in embryogenesis. Plant J **41**: 125–132

Takahashi H, Saito Y, Kitagawa T, Morita S, Masumura T, Tanaka K (2005) A novel vesicle derived directly from endoplasmic reticulum is involved in the transport of vacuolar storage proteins in rice endosperm. Plant Cell Physiol **46**: 245–249

Takemoto Y, Coughlan SJ, Okita TW, Satoh H, Ogawa M, Kumamaru T (2002) The rice mutant *esp2* greatly accumulates the glutelin precursor and deletes the protein disulfide isomerase. Plant Physiol **128**: 1212–1222

Tanaka K, Sugimoto T, Ogawa M, Kasai Z (1980) Isolation and characterization of two types of protein bodies in the rice endosperm. Agric Biol Chem **44**: 1633–1639

Ueda T, Yamaguchi M, Uchimiya H, Nakano A (2001) Ara6, a plant-unique novel type Rab GTPase, functions in the endocytic pathway of Arabidopsis thaliana. EMBO J **20**: 4730–4741

Uemura T, Ueda T (2014) Plant vacuolar trafficking driven by RAB and SNARE proteins. Curr Opin Plant Biol **122**: 116–121

Wang JQ, Tse YC, Hinz G, Robinson DG, Jiang LW (2012) Storage globulins pass through the Golgi apparatus and multivesicular bodies in the absence of dense vesicle formation during early stages of cotyledon development in mung bean. J Exp Bot **63**: 1367–1380

Wang Y, Liu F, Ren Y, Wang Y, Liu X, Long W, Wang D, Zhu J, Zhu X, Jing R et al. (2016) GOLGI TRANSPORT 1B regulates protein export from the endoplasmic reticulum in rice endosperm cells. Plant Cell **28**: 2850–2865

Wang Y, Ren Y, Liu X, Jiang L, Chen L, Han X, Jin M, Liu S, Liu F, Lv J, et al. (2010) OsRab5a regulates endomembrane organization and storage protein trafficking in rice endosperm cells. Plant J **64**: 812–824

Wang Y, Zhu S, Liu S, Jiang L, Chen L, Ren Y, Han X, Liu F, Ji S, Liu X, Wan J (2009) The vacuolar processing enzyme OsVPE1 is required for efficient glutelin processing in rice. Plant J **58**: 606–617

Wu XX, Ebine K, Ueda T, Qiu QS (2016) AtNHX5 and AtNHX6 are required for the subcellular localization of the SNARE complex that mediates the trafficking of seed storage proteins in Arabidopsis. Plos One **11**: e0151658

Yamagata H, Sugimoto T, Tanaka K, Kasai Z (1982) Biosynthesis of storage proteins in developing rice seeds. Plant Physiol **70**: 1094–1100

Yamagata H, Tanaka K (1986) The site of synthesis and accumulation of rice storage proteins. Plant Cell Physiol **27**: 135–145

Yang X, Gong P, Li KY, Huang FD, Cheng FM, Pan G (2016) A single cytosine deletion in the OsPLS1 gene encoding vacuolar-type H^+-ATPase subunit A1 leads to premature leaf senescence and seed dormancy in rice. J Exp Bot **67**: 2761–2776

Zhang HY, Niu XL, Liu J, Xiao FM, Cao SQ, Liu YS (2013) RNAi-directed downregulation of vacuolar H^+-ATPase subunit A results in enhanced stomatal aperture and density in rice. Plos One **8**: e69046

Zhou AM, Bu YY, Takano T, Zhang XX, Liu SK (2016) Conserved V-ATPase c subunit plays a role in plant growth by influencing V-ATPase-dependent endosomal trafficking. Plant Biotechnol J **14**: 271–283

Zhu J, Ren Y, Wang Y, Liu F, Teng X, Zhang Y, Duan E, Wu M, Zhong M, Hao Y, et al. (2019) OsNHX5-mediated pH homeostasis is required for post-Golgi trafficking of seed storage proteins in rice endosperm cells. BMC Plant Biol **19**: 295